ISSN 0965-5441, Petroleum Chemistry, 2017, Vol. 57, No. 13, pp. 1207–1218. © Pleiades Publishing, Ltd., 2017.
Original Russian Text © E.D. Belashova, O.A. Kharchenko, V.V. Sarapulova, V.V. Nikonenko, N.D. Pismenskaya, 2017, published in Membrany i Membrannye Tekhnologii, 2017, Vol. 7, No. 6, pp. 384–397.

Effect of Protolysis Reactions on the Shape of Chronopotentiograms of a Homogeneous Anion-Exchange Membrane in NaH_2PO_4 Solution

E. D. Belashova*, O. A. Kharchenko, V. V. Sarapulova, V. V. Nikonenko, and N. D. Pismenskaya

Kuban State University, Krasnodar, 350040 Russia

**e-mail: ekaterinabelashova23@gmail.com*

Received June 11, 2017

Abstract—Single-pulse and double-pulse chronopotentiograms of a homogeneous anion-exchange membrane AX in 0.02 M solutions of NaCl (system 1) or NaH_2PO_4 (system 2) have been recorded in underlimiting and overlimiting current modes. It has been found that in the case of exceeding the limiting current ($i > i_{lim}^{Lev}$) calculated using the convection–diffusion model, the time required to establish a steady state in system 2 increases by more than an order of magnitude compared to system 1. The slow growth of the potential drop is due to a gradual transition of the membrane from the form in which the main counterion is $H_2PO_4^-$ to the HPO_4^{2-} form. This transition is due to the deprotonation of a part of $H_2PO_4^-$ ions forming HPO_4^{2-} and protons as they enter the membrane. The participation of H^+ in charge transfer in the depleted diffusion layer at a given current density causes a lower value of the potential drop than in system 1 for the same i/i_{lim}^{Lev} ratio. In intense current regimes, chronopotentiograms of system 2 exhibit two inflection points. The first point corresponds to the classical Sand transition time and is due to reaching the limiting current of $H_2PO_4^-$ ions (the main charge carrier for $i < i_{lim}^{Lev}$) in the depleted diffusion layer. The second point is associated with a critical current that can be called the second limiting current in the system with NaH_2PO_4 and has no analogue in the system with NaCl. This current, which is approximately $2i_{lim}^{Lev}$, corresponds to the state when the membrane is completely transformed into the HPO_4^{2-} form. Meanwhile, the source of protons due to the transformation of $H_2PO_4^-$ into HPO_4^{2-} ions as they enter the membrane is exhausted. After reaching this critical value of the potential drop, either the HPO_4^{2-} deprotonation reaction to give triply charged PO_4^{3-} ions in the membrane or the water splitting on fixed groups located at the membrane/solution interface may occur.

Keywords: anion-exchange membrane, ampholyte, two-pulse chronopotentiometry, intradiffusion kinetics, concentration profiles, protonation–deprotonation reactions

DOI: 10.1134/S0965544117130035

INTRODUCTION

Electromembrane purification, separation, conditioning, and concentration processes in combination with other membrane methods are actively introduced into the food and pharmaceutical industry [1], as well as in the production of nutrients for the livestock industry [2]. This rapidly developing line is based on the concentration, demineralization, and fractionation of ampholyte-containing liquid media, whose source is the products of biochemical processing of biomass and organic waste [3]. Ampholytes can contain both acidic and basic groups, which enter protonation/deprotonation reactions in aqueous solutions. Therefore, the charge of ampholyte particles depends on the pH of the medium. This feature leads to the appearance of membrane transport mechanisms that are not observed in the case of strong electrolytes, such as NaCl. The barrier and circulation effects in the transfer of ampholyte particles in the electrodialysis desalting compartment are described in the literature [4, 5], as well as the phenomena of facilitated diffusion [6] and electrodiffusion [7] through an ion-exchange membrane (IEM). All of these effects are associated with the transformation of one ampholyte form into another with a local change in pH. The barrier and circulation effects take place in the intermembrane space of the desalting compartment of an electrodialysis device. The source of protons or hydroxyl ions, which participate in the protonation–deprotonation reactions of ampholytes in a depleted diffusion layer (DL), is water splitting at the IEM/solution interface in overlimiting current regimes. Facilitated diffusion and electrodiffusion of amino acids [6–8] and/or inor-

ganic ampholytes, for example, single-charged phosphoric acid anions [9] occur inside an IEM. There have been studies [4–9] considering the case where protons or hydroxyl ions responsible for a change in the ampholyte charge enter a membrane via its preliminary conversion into the relevant ionic form [6, 8] or as a product of water splitting at the IEM/solution interfaces in overlimiting current regimes [7]. At the same time, the change in the electric charge of ampholytes in the internal solution of IEM relative to the external solution can also be due to another cause. It is the Donnan exclusion of H^+ and OH^- ions as coions with a decrease in the concentration of the external solution bordering the membrane [10–12]. It is known [13] that the Donnan exclusion effect is enhanced with dilution of the external solution. When an external electric field is applied to the membrane system, the ampholyte concentration in the depleted DL decreases. Thus, the composition of the internal solution of the membrane becomes a function of the current density.

In this paper we will consider how changes in the internal solution of the membrane affect both the time of establishment of a quasi-equilibrium state and the shape of chronopotentiograms under intense current regimes. To this end, we will analyze the double-pulse chronopotentiograms of a homogeneous anion-exchange membrane (AEM) in a 0.02 M NaH_2PO_4 solution and compare them with those obtained in a NaCl solution. The AEM composition and the shape of concentration profiles in the diffusion layers will be calculated using a quasi-steady-state, three-layer 1D model.

EXPERIMENTAL

Objects of Study

The object of the study was a homogeneous anion-exchange membrane AX, which mainly contains fixed quaternary ammonium groups. The total exchange capacity of the swollen membrane in the Cl^- form is 1.95 ± 0.03 mol/L. Its thickness in the swollen state is 170 ± 10 μm. The membrane was studied in 0.02 M solutions of NaCl and NaH_2PO_4. The solutions were prepared using distilled water having an electrical resistance of 400 kΩ cm and pH 5.5 and the analytical-grade chemicals (Vekton, St. Petersburg, Russia).

The specific electrical conductivity of the membrane in solutions of sodium salts of hydrochloric and orthophosphoric acids was determined by a differential method using a clip cell [14] and a Motech MT4080 inductance/capacitance/resistance meter at a frequency of 10 kHz and a temperature of 25°C.

Procedure for Recording Experimental Chronopotentiograms

Chronopotentiograms (ChPs) of the membrane were obtained using the setup sketched in Fig. 1a. The geometry of the flat slit channels of the electrochemical cell is formed by ion-exchange membranes and plexiglas frames (Fig. 1b) separated by paraffin film, which have square holes of a 2.0×2.0 cm^2 size. The intermembrane distance (h) is 0.67 cm, and the length of the channels (L) is 2 cm. The plexiglas frames are equipped with special feed-solution inlet and outlet devices, which provide a laminar flow regime of the fluid. The AOM* under study forms a desalting channel in a couple with a heterogeneous cation-exchange membrane MK-40 (Shchekinoazot, Russia). Two Luggin glass capillaries connected to silver/silver chloride electrodes were used to measure the potential drop (PD). The tips of the capillaries had an inner diameter of about 0.8 mm. The distance between them and the AEM surface was about 1 mm. Simultaneously with ChP recording, the pH the solution at the inlet and outlet of the desalting compartment under study were measured. The design of the flow-through four-compartment electrochemical cell, the schematic of the setup, and the procedures for measuring and processing the resulting kinetic relations of the potential drop and pH are detailed in [15, 16]. All the experiments were performed at a constant temperature of 25 ± 1°C.

Prior to the experiments, all the membranes were subjected to standard salt pretreatment [17]. Then, each of them was divided into two samples. One of the samples was equilibrated with a 0.02 M NaCl solution, and the other with a 0.02 M NaH_2PO_4 solution.

In preliminary experiments using single-pulse chronopotentiometry, it was found that the time of concentration profiles formation in the studied membrane system does not exceed 30–40 min. Proceeding from the fact that the relaxation processes should take approximately the same time, the membrane system was maintained at zero current and continuous pumping of the feed solution for at least 30 min after each application of an electric current.

The interval between the 1st and 2nd current pulses was 60 s in all cases, unless otherwise stated, and a current through the studied membrane during the pause was zero. Chronopotentiograms were obtained with the horizontal position of the membrane stack, when the depleted DL is located under the studied membrane and gravitational convection does not arise at its surface.

Calculation of Theoretical Values for Electrochemical-System Characteristics

The maximum current density along the channel length can be calculated using the Lévêque equation obtained in terms of the convection–diffusion model

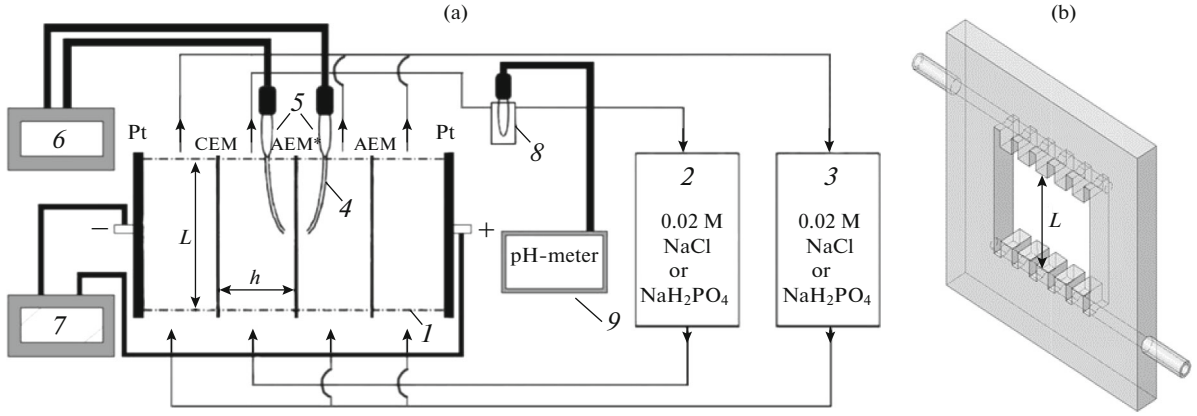

Fig. 1. (a) Schematic of the experimental setup and (b) an image of one of the plexiglas frames that form the channels of a flow-through electrochemical cell (*1*) used to record chronopotentiograms of a membrane; Pt stands for flat polarizing platinum electrodes, AEM* is the studied anion-exchange membrane, AEM and CEM are the auxiliary cation-exchange (MK-40) and anion-exchange (MA-41) membranes, respectively; (*2*, *3*) containers with 0.02 M feed solution; (*4*) Luggin capillaries; (*5*) vessels in which closed silver/silver chloride electrodes are inserted; (*6*, *7*) potential drops recording and current setting units of an Autolab PGStat-100 electrochemical workstation; (*8*) flow-through microcell with a combined pH measuring electrode; (9) Mettler Toledo Five Easy Plus FEP20 pH meter.

of ion transport [18] and adapted to the plane channels formed by ion-exchange membranes

$$i_{\lim}^{\mathrm{Lev}} = 1.47 \times \frac{FDz_1C_1}{h(T_1 - t_1)}\left(\frac{h^2V}{LD}\right)^{1/3}, \qquad (1)$$

where z_1 is the charge number of the counterion, C_1 is its concentration in the solution at the inlet to the desalting channel, D is the diffusion coefficient of the electrolyte, L is the length of the desalting channel, h is the intermembrane distance, V is the average linear flow velocity of the solution, T_1 is the effective transport number of the counterion in the membrane, t_1 is the electromigration transport number of that ion in solution, and F is Faraday's number. The values of the limiting current density ($i_{\lim}^{\mathrm{Lev}}$) calculated by Eq. (1) are 3.1 mA cm^{-2} (in 0.02 M NaCl) and 1.6 mA cm^{-2} (in 0.02 M NaH_2PO_4). The channel length-averaged DL thicknesses found by combining Eq. (1) with the Peers equation [13] are 254 μm (NaCl) and 224 μm (NaH_2PO_4). The following values of the parameters were used in the calculations: $D = 1.6 \times 10^{-5}$ cm^2/s, $t_1 = 0.604$, $T_1 = 1$ (system AX/NaCl solution); $D = 1.1 \times 10^{-5}$ cm^2/s, $t_1 = 0.419$, $T_1 = 1$ (system AX/NaH_2PO_4 solution). As in the case of the convection–diffusion model [19] taking into account the presence of diffusion, migration, and convective components, the Peers equation was derived on the assumption that the only charge carriers in the membrane system under consideration are the salt cations and anions and the condition of local electroneutrality is also satisfied.

The values of the transition time τ_{Sand} were estimated using the Sand equation obtained in terms of the semi-infinite diffusion theory [20]:

$$\tau_{\mathrm{Sand}} = \left(\frac{\pi D}{4}\right)\left(\frac{C_1 z_1 F}{T_1 - t_1}\right)^2 \frac{1}{i^2}, \qquad (2)$$

where i is the set current density. These calculations were made on the assumption that the dominant counterion in the depleted DL is the dihydrogen phosphate anion $H_2PO_4^-$ (AX/NaH_2PO_4 solution system) or the chloride ion Cl^- (AX/NaCl solution system).

Mathematical Modeling of Transport of Sodium Dihydrogen Phosphate Ions through Anion-Exchange Membrane

Concentration profiles in the membrane AX and adjacent diffusion layers under conditions of attained thermodynamic equilibrium were calculated in terms of a 1D three-layer, steady-state transfer model [21]. The model uses the assumption that the ampholyte protonation–deprotonation reactions occur both inside the membrane and in the solution in boundary diffusion layers with a given thickness; ion-exchange equilibrium between the compositions of the membrane and the adjacent solution is observed. The model considers a three-layer system consisting of a membrane and adjacent diffusion layers during the flow of a direct current. Migration and diffusion transport of particles in all the three layers are taken into account. It is supposed that all the salts of orthophosphoric acid are in the completely dissociated state and there are no interionic interactions between molecules of orthophosphoric acid and/or its anions. The model is based on the Nernst–Planck equation; chemical equilibrium equations; and the conditions of continuity of the electric current density passing through the membrane system, local electroneutrality, and preser-

vation of the constant total flux of orthophosphoric acid anions.

The calculations were carried out using the following parameters of the membrane system. The concentration of sodium dihydrogen phosphate in the bulk solution was taken to be 0.02 mol/L; pH 4.7. The first-, second-, and third-step equilibrium constants of the protonation–deprotonation reactions of phosphoric acid and the water autoprotolysis constant are respectively [22] $K_{a,1} = 7.25 \times 10^{-3}$ mol/L ($pK_{a,1} = 2.12$), $K_{a,2} = 6.31 \times 10^{-8}$ mol/L ($pK_{a,2}$ 7.21), $K_{a,3} = 4.8 \times 10^{-13}$ mol/L ($pK_{a,3} = 12.34$), and $K_b = 10^{-14}$ mol/L (pK_b 14). The diffusion coefficients of ions and molecules at infinite dilution are as follows [23]: $D_0 = 0.91 \times 10^{-5}$ cm^2/s (H_3PO_4), $D_1 = 0.958 \times 10^{-5}$ cm^2/s ($H_2PO_4^-$), $D_2 = 0.759 \times 10^{-5}$ cm^2/s (HPO_4^{2-}), $D_3 = 0.824 \times 10^{-5}$ cm^2/s (PO_4^{3-}), $D_4 = 5.27 \times 10^{-5}$ cm^2/s (OH^-), $D_5 = 9.3 \times 10^{-5}$ cm^2/s (H^+), and $D_6 = 1.334 \times 10^{-5}$ cm^2/s (Na^+).

Determining the exact values of diffusion coefficients in a membrane is a very difficult task for a multicomponent system. For a rough estimate, we note that the size of orthophosphoric acid anions (which are counterions for anion-exchange membranes) differ insignificantly. Therefore, it can be assumed that the diffusion coefficients of all these ions have close values. These diffusion coefficients can be approximately estimated at $\bar{D}_i = 2 \times 10^{-11}$ m^2/s. The membrane conductivity calculated using these diffusion coefficients is 0.98 mS/cm, which agrees with the experimentally determined value of 1.0 mS/cm [24].

RESULTS AND DISCUSSION

Figures 2–4 show the chronopotentiograms obtained for the AX membrane in 0.02 M NaCl or NaH_2PO_4 solutions. In the NaCl solution, the ChP shape for the first (ChP-1) and for the 2nd (ChP-2) current pulses is almost identical (Fig. 2a) and does not differ from that described in many papers [15, 25]. It has three segments: the "ohmic" section (I) corresponding to an instantaneous potential drop due to switching on the current; the one of the potential drop growth caused by an increase in the concentration polarization of the membrane system and the formation of concentration profiles in the DL of the solution (II), and the section of entering into a steady state (III). At currents below the limiting current ($i < i_{lim}^{Lev}$), the potential drop in segment II increases monotonically (Figs. 2a, 2b); the values of the PD derivative with respect to time slowly decreases; and the curve does not contain extremum points (Fig. 2c), thereby indicating that there are no inflection points on it. At $i > i_{lim}^{Lev}$, this section of the chronopotentiogram exhibits an inflection (point *b* in Figs. 2a, 2b), which corresponds to a local maximum on the PD derivative with respect to time (Fig. 2c). The inflection is due to the appearance of new current transport mechanisms complementary to the diffusion and migration of counterions, when the electrolyte concentration near the membrane surface reaches a certain sufficiently small threshold value. This can be current-induced convection (electroconvection and/or gravitational convection) [15, 28], as well as the generation of new charge carriers, H^+ and OH^- ions. When a new transport mechanism comes into play, the potential drop growth rate decreases with time and the system gradually passes to a steady state.

The values of the ohmic ($\Delta\varphi_{Ohm}$) and steady-state ($\Delta\varphi_{st}$) potential drops are determined at points a and c. In the case when there is no intense electroconvection and the current density is high enough ($i/i_{lim}^{Lev} \geq 1.7$ [26]), the values of the transition time found at point *b* on the experimental ChP (τ_{exp}) coincide within the error of its determination with the value calculated by Eq. (2) (Fig. 2c). The reason for the possible deviation of experimental values τ_{exp} from the value calculated by Eq. (2) is the finite thickness of the DL. At the outer boundary of the DL, the concentration is replenished by forced convection, which leads to a delay in the formation of the profile and an increase in the transition time compared with the Sand theory, in which the DL thickness is assumed to be infinitely large. At high currents, the concentration profile is formed rapidly and conditions on the outer boundary of the DL do not affect the transition time. At low currents, the Sand conditions on the DL outer boundary are not satisfied, and Eq. (2) gives an underestimated value of τ [26].

The time for formation of concentration profiles after switching on the current is approximately equal to the time of their disappearance/dissipation when the current is turned off. In the current range examined, it does not exceed 30 s. Therefore, regardless of whether the second dc pulse is applied in 30 s (ChP-2') or 60 s (ChP-2), the shapes of these curves are almost identical (Fig. 2a), the transition times found for the ChPs have close values (Fig. 2c), and the initial parts of corrected ChP-1 and ChP-2 (the ohmic component is subtracted from the current ChP value [16], $\Delta\varphi' = \Delta\varphi - \Delta\varphi_{Ohm}$) differ little from each other (Fig. 2b). The time for establishing the quasi-steady state, τ_{st}, which corresponds to point c on the ChP and the potential drop $\Delta\varphi_{st}$ (Fig. 2a), is determined by external diffusion kinetics and amounts to several tens of seconds. In an overlimiting current regime, the value of τ_{st} decreases with increasing i/i_{lim}^{Lev}.

The water splitting at the membrane/solution interface is a result of protonation–deprotonation reactions of fixed groups involving water molecules and is stimulated by a high electric field strength achieved in overlimiting current regimes [27]. High field strength ensures elongation of H–OH bonds and

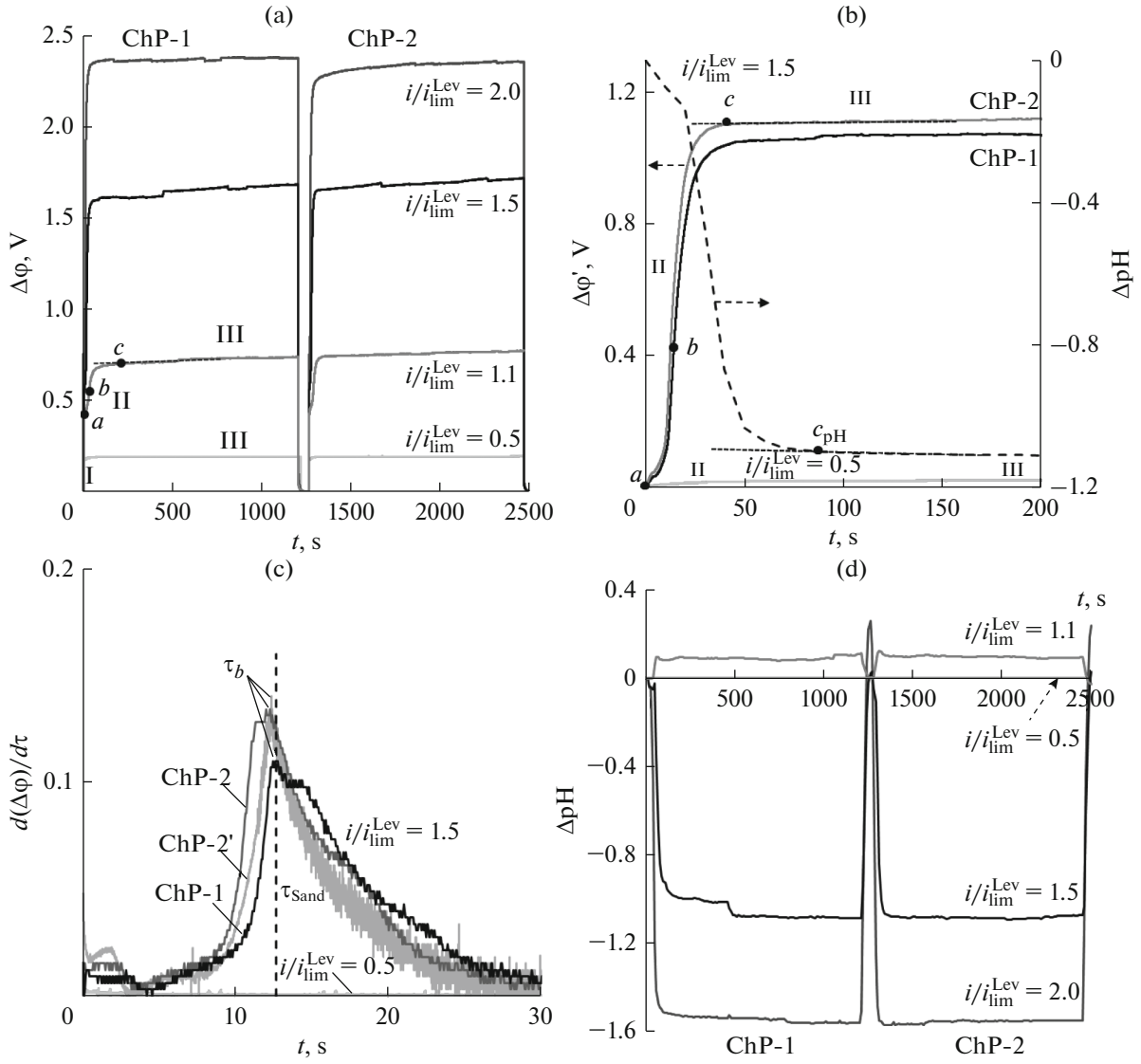

Fig. 2. (a) Two-pulse chronopotentiograms of the AX membrane in a 0.02 M NaCl solution; (b) initial parts of the corrected chronopotentiograms of the first (ChP-1) and the second (ChP-2) direct-current pulses; (c) the same curves in the differential form at $i/i_{lim}^{Lev} = 1.5$ and $i/i_{lim}^{Lev} = 0.5$; and (d) the corresponding (to the ChPs) difference in pH at the outlet and inlet of the desalting compartment formed by the membrane AX and the auxiliary membrane MK-40. The pause ($i = 0$) between the fist and the second current pulse is 30 s (ChP-2') or 60 s (ChP-2).

a continuous withdrawal of H^+ and OH^- ions from the reaction zone. For the contribution to the pH by water splitting at the interface to be noticeable, the concentration of salt ions at the interface must be on the order of 10^{-5} mol/L (then the transport number of the water splitting products will be about 0.1 with taking into account the fact that the mobility of these ions is about an order of magnitude greater than that of the salt ions). According to previous estimates [28, 29], the generation of these ions at the homogeneous membrane/solution interface can begin if $\Delta\varphi' \geq 0.3$ V. In the AX/NaCl solution system at $i/i_{lim}^{Lev} = 1.1$, the maximum (steady-state) value is $\Delta\varphi' = 0.28$ V; that is, the threshold value of 0.3 V is not exceeded. Under these conditions, H^+ and OH^- ions are generated predominantly at the surface of the auxiliary cation-exchange membrane, causing alkalization of the solution at the exit from the desalting compartment (Fig. 2d). At higher current densities when the threshold value $\Delta\varphi'$ is reached, the desalting solution is acidified (Fig. 2d), indicating more active water splitting at the AX/NaCl solution interface compared to that at the cation-exchange membrane boundary. Figure 2d allows closer examination of the relation between the water splitting and the shape of ChP for the AX/NaCl solution system at $i/i_{lim}^{Lev} = 1.5$. Indeed, a noticeable shift in

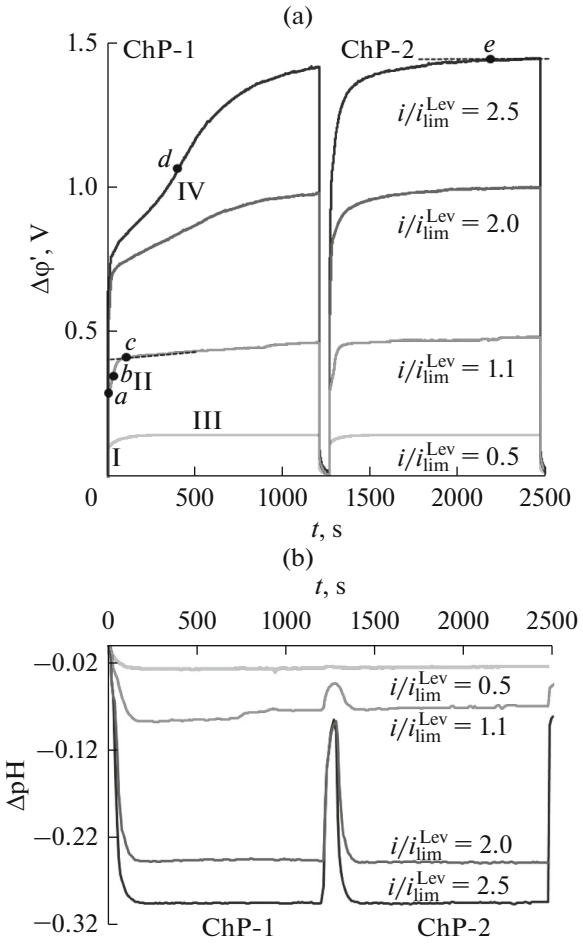

Fig. 3. (a) Two-pulse chronopotentiograms of the AX membrane in a 0.02 M NaH_2PO_4 solution and (b) the corresponding (to these chronopotentiograms) difference in pH at the outlet and inlet of the desalting channel formed by the membrane AX and the auxiliary membrane MK-40.

pH to the acidic side (by about 0.1 pH units) is observed 20 seconds after the onset of current flow, when the value of Δφ' reaches 0.3 V. The same trend is observed at other current densities. The steady-state value of ChP is reached somewhat faster (60 s) than steady-state pH values are established (75 s).

In the AX/NaH_2PO_4 solution system, ChP-1 and ChP-2 are almost identical in the current range of $0.5 < i/i_{lim}^{Lev} \le 1.1$ (Figs. 3a, 4). Their form does not differ significantly from that recorded in the AX/NaCl solution system. However, there are significant differences at currents above the limiting current. The main thing is that it takes tens of minutes to achieve a steady state, not dozens of seconds as in the case of NaCl. The initial part of the chronopotentiogram for the AX/NaH_2PO_4 solution system (Fig. 4b) in the case of application of the first current pulse (ChP-1) qualitatively agrees with that for the AX/NaCl solution system (Fig. 2b): the potential rapidly grows and, at $i > i_{lim}^{Lev}$, the curve exhibits an inflection point b corresponding to the transition time τ_{exp}. Despite the fact that the inflection point in the initial part of the ChP in the AX/NaH_2PO_4 solution system is less pronounced than in the AX/NaCl solution system, the value of τ_{exp} is in good agreement with the transition time τ_{Sand} calculated by Eq. (2) (Fig. 4b). Approximately 10 seconds after reaching the transition time, ChP-1 (Fig. 4b) flattens out (plateau between points *c* and *c*') as in the NaCl solution. However, the further course of ChP-1 significantly differs from the curves observed in the AX/NaCl solution system. Growth of the PD between points *c*' and *e* is recorded. The constant values of the potential drop (segment V) are reached after a time exceeding 1200 s. An interesting feature is that over a certain critical current density, ChP-1 in the case of NaH_2PO_4 displays an inflection point d similar to the one that appears at times close to τ_{Sand}. Note that the repeated application of a dc pulse after a pause of 60 seconds leads to chronopotentiogram ChP-2, which is noticeably different from ChP-1 (Figs. 3, 4). The potential drop on ChP-2 grows much faster than on ChP-1; the inflection points in segments II and IV disappear, and the time of establishment of a quasi-equilibrium PD is significantly (by a factor of 4 to 5) corrected in comparison with the first pulse.

Note that slight acidification of the desalting solution in the AX/NaH_2PO_4 solution systems is observed already in the underlimiting current regime (Fig. 3b) at potential drops well below the threshold value of $\Delta\varphi' = 0.3$ V. At $i/i_{lim}^{Lev} \ge 1$, it increases with increasing current (Fig. 3b), but the pH changes are much smaller than those observed in the NaCl solutions (Fig. 2d).

To understand the possible causes of the difference in the ChP form between the membrane systems in NaCl and NaH_2PO_4 solutions, let us analyze the results of calculations of the concentration profiles of the solution components during the flow of electric current in the AX membrane/NaH_2PO_4 solution system (Fig. 5).

A characteristic feature of the behavior of the system is that the contribution of different charge carriers varies with a change in current density. Due to the Donnan exclusion of protons, the coions, from the membrane, the pH of the internal solution is shifted to the alkaline side relative to the outer solution [10, 13]. By crossing the interphase boundary, $H_2PO_4^-$ ions get from a more acidic medium into a more alkaline medium. The result is the deprotonation of part of these ions to give rise to doubly-charged anions in the membrane and the release of H^+ ions (hydroxonium ions H_3O^+), which return to the depleted solution:

$$H_2PO_4^- + H_2O \Leftrightarrow HPO_4^{2-} + H_3O^+. \quad (3)$$

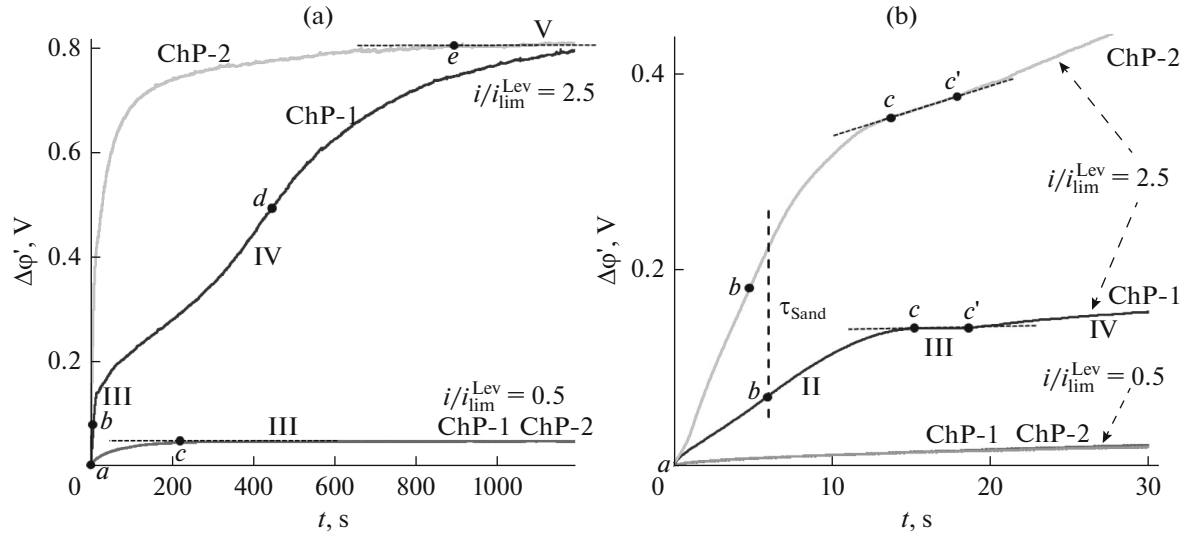

Fig. 4. (a) Two-pulse chronopotentiograms of the AX membrane in a 0.02 M NaH_2PO_4 solution and (b) their initial parts. The dashed line shows the transition time, τ_{Sand}, calculated by Eq. (2).

As the electrolyte concentration in the depleted solution at the membrane surface (C_s) decreases, the pH of the boundary internal solution increases, because the effect of Donnan exclusion of protons is enhanced. Since C_s decreases with increasing current, the equilibrium of reaction (3) progressively shifts to the right; that is, an increasing number of singly charged $H_2PO_4^-$ ions convert to doubly charged HPO_4^{2-} ions when crossing the boundary and an increasing number of H^+ ions are generated at the interface. Similar effects were discussed in a study [30] on the transport of amino acids in systems with ion-exchange membranes in an applied electric field.

The results of calculations for the membrane system under the established equilibrium conditions show that at currents below the limiting value (case of $i/i_{lim}^{Lev} = 0.5$ in Fig. 5a), C_s is comparable in value to the electrolyte concentration in the bulk solution, C_b. The rate of generation of H^+ ions at the interface is low; therefore, the concentration of H^+ ions in the depleted DL is small (Fig. 5a), and actually the only charge carriers in this diffusion layer are $H_2PO_4^-$ anions.

Inside the membrane, these anions dominate, but about 5% of the electric charge is transferred by HPO_4^{2-} ions. An increase in current density to values of $i/i_{lim}^{Lev} = 1.1$ (Fig. 5b) leads to a significant decrease in C_s ($C_s = 8 \times 10^{-2} C_b$), which stimulates additional Donnan exclusion of protons from the near-surface layer of the membrane. As a result, the pH of the internal solution rises to 6.8 (AX/depleted DL interface) and 7.4 (AX/enriched DL interface, the concentration of ions in it increases, and their contribution in charge transport inside the membrane reaches 27%. The number of protons entering the depleted DL increases, but their contribution to charge transport still remains insignificant compared to $H_2PO_4^-$ anions, being 15%. At a current of $i/i_{lim}^{Lev} = 2.0$ (Fig. 5c), $C_s = 4 \times 10^{-4} C_b$. The propart of HPO_4^{2-} ions involved in charge transport inside the membrane increases to 90%. In the depleted DL, protons transfer up to 49% of the charge. Inside this layer, the concentration profiles of protons and orthophosphoric acid produced by protonation of HPO_4^{2-} are formed (Fig. 5c). A further increase in the current density (Fig. 5d) leads to a subsequent decrease in C_s and a nearly complete conversion of the bulk membrane into the form of doubly charged anions. In that case, a certain critical current is achieved, which can be called the second limiting current in the AX/NaH_2PO_4 solution system. It is due to the fact that the increase in the potential drop in a certain interval of values after the complete conversion of the membrane into the HPO_4^{2-} form is accompanied neither by the appearance of new charge carriers nor by significant enhancement of coupled convection. As a result, there is acceleration of the potential drop growth observed in segment IV up to the inflection point d of ChP-1 (Fig. 4). This point corresponds to the appearance of additional charge carriers in the depleted DL. These can be protons that are generated in the membrane layer bordering the depleted DL as a result of deprotonation of HPO_4^{2-} anions to give triply charged PO_4^{3-} anions or as a result of protonation–deprotonation reactions of fixed membrane groups to yield OH^- anions, which are transported through the membrane. For the appearance of the triply charged

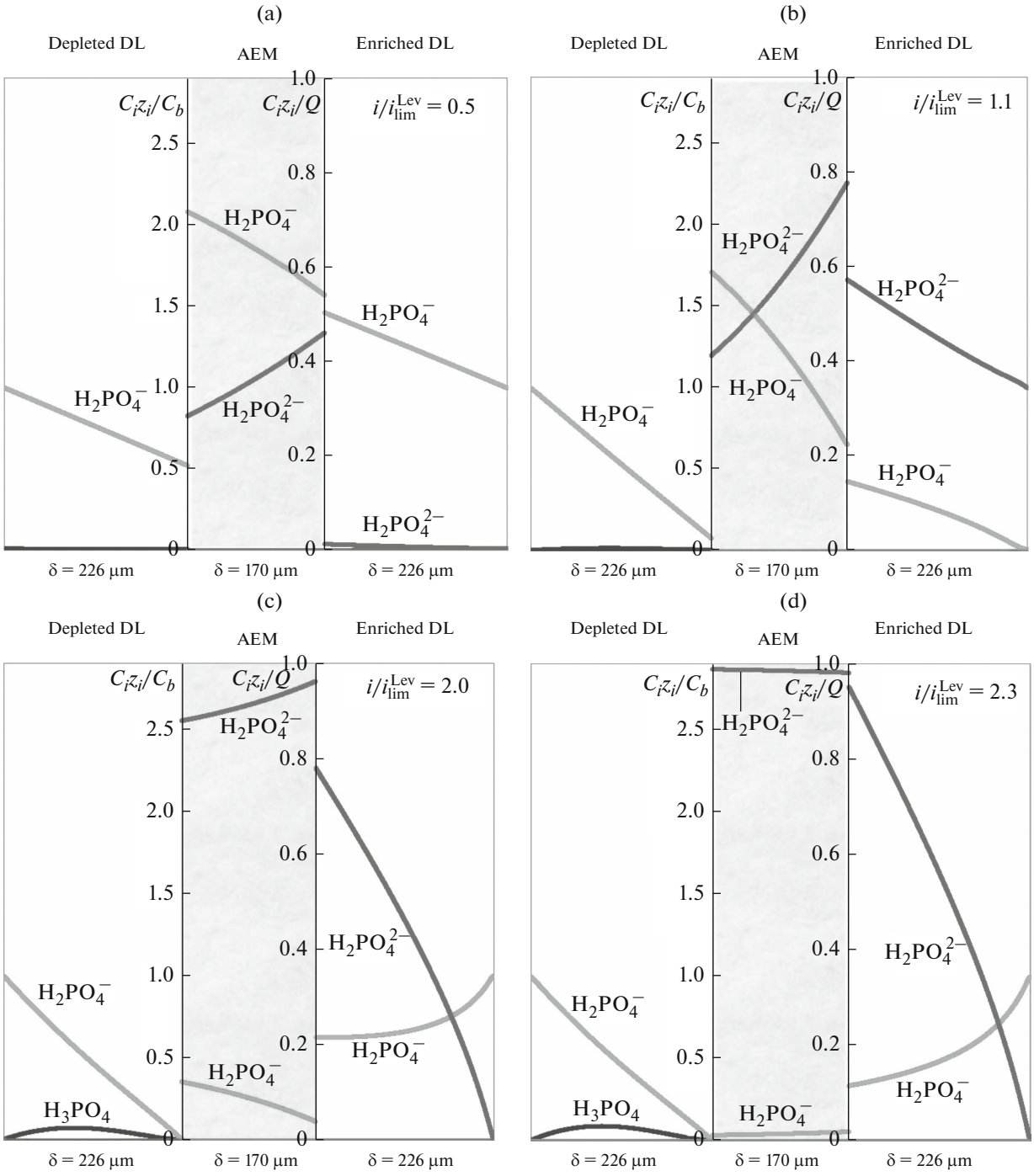

Fig. 5. Dimensionless concentration profiles of individual components of the NaH_2PO_4 solution in the anion-exchange membrane AX and the adjacent diffusion layers in a steady state at a current density i/i_{lim}^{Lev}: of (a) 0.50, (b) 1.00, (c) 2.00, or (d) 2.25. Equivalent concentrations z_iC_i are used in the case of ions, and molar concentration C_i is used for neutral phosphoric acid molecules.

ions in the membrane, the pH of the internal solution should become as high as 10.2. To this end, the value of C_s should decrease to $4 \times 10^{-6}C_b$. Therefore, most likely, the source of protons is primarily the fixed groups located on the AX/depleted DL boundary. However, this assumption requires additional research. Regarding the coupled convection, the development of intense unstable convection via the

Rubinstein and Zaltzman mechanism [31] requires a potential drop in the depleted DL to be about 1 V, whereas the measured value of $\Delta\varphi'$ at $i/i_{lim}^{Lev} = 2.5$ is approximately 0.8 V (Fig. 4a). Such a low value of the potential drop is due to a high concentration of H^+ ions in the depleted DL.

The above analysis allows us to propose the following interpretation of the ChP form for the system AX/NaH_2PO_4 solution. At short times, no more than two to three times the Sand transition time, the phenomena occurring in this system differ little from those in the AX/NaCl solution system. Immediately after the initial ohmic PD, the potential growth is due to a decrease in the concentration of the NaH_2PO_4 electrolyte in the depleted DL. The main charge carriers are the $H_2PO_4^-$ ions. If the current does not exceed the limiting value for these ions, the PD reaches a constant value without inflections on the ChP, as in the case of NaCl. If $i/i_{lim}^{Lev} > 1$, the electrolyte concentration at the membrane surface C_s decreases to sufficiently small values at which a new transport mechanism arises: the generation of H^+ ions (reaction (3)) to be transferred to the bulk of the depleted DL. The appearance of the new charge carriers in the depleted DL results in that the growth of $\Delta\varphi$ slows down and the system reaches a quasi-steady state (segment III on ChP). However, unlike the case of NaCl, this state is not steady: a small plateau (segment III) in the ChP of the AX/NaH_2PO_4 solution system is followed by PD growth (part VI, Figs. 3, 4). This slow growth is due to the rearrangement of the concentration profiles of the $H_2PO_4^-$ and HPO_4^{2-} ions within the membrane. Deprotonation of $H_2PO_4^-$ ions upon their entry into the membrane in accordance with reaction (3) leads to an increase in the concentration of HPO_4^{2-} ions in the internal solution of the membrane at the boundary with the depleted DL. Accordingly, the concentration of $H_2PO_4^-$ ions at this boundary decreases in comparison with their concentration at the opposite boundary of the membrane. The rate of arrival of protons in the depleted DL, which largely determines the potential drop recorded on the ChP, depends on the rate of rearrangement of these concentration profiles. Evaluating the time of this process using the well-known relation $t = d^2/D$ [32], where the membrane thickness is $d = 1.7 \times 10^{-2}$ cm and the mutual diffusion coefficient estimated from the values of electrical conductivity is $D = 2 \times 10^{-7}$ cm^2/s, gives the order of 10^3 s. Our experiments show the same order (3000–4000 s) for the time of establishing a constant rate of arrival of protons at distilled water if the anion-exchange membrane, preliminarily equilibrated with a NaH_2PO_4 solution, is placed between this solution and distilled water ($i = 0$) [33]. Such an experiment simulates the situation when the near-surface concentration of $H_2PO_4^-$ ions in the depleted DL decreases to values close to zero as a result of concentration polarization in the AX/NaH_2PO_4 solution system. The only difference is that the migration component is added to the diffusion mechanism of the rearrangement of these profiles when an electric field is applied. Therefore, in the case of chronopotentiometry, the quasi-steady state in the AX/NaH_2PO_4 solution system is reached faster.

It should be noted that the ChP of the AX/NaH_2PO_4 solution system does not exhibit an inflection point d at $i < 2i_{lim}^{Lev}$ and such a point appears at a time of about 500 s at current densities of $i > 2i_{lim}^{Lev}$. The PD rise before the inflection point *d* is apparently due to the attainment of a state where the membrane surface layer facing the depleted solution completely transforms into the form of doubly charged HPO_4^{2-} anions. Reaching the maximum concentration of these ions in the membrane means saturation of the stream of H^+ ions entering the depleted DL.

After reaching the critical value of the potential drop corresponding to point *d*, either the reaction of deprotonation of HPO_4^{2-} anions in the membrane to give triply charged PO_4^{3-} ions or the water splitting on fixed groups located at the membrane/solution interface can begin. It is the appearance of these additional charge carriers in the membrane and the additional amount of protons generated in the depleted DL that is responsible for the subsequent slowing of PD growth and the tendency to achieve a constant value of $\Delta\varphi_{st}$.

A short-term (60 s) current shutdown leads to smearing (disappearance, relaxation) of the concentration profiles of ions in the depleted DL. But this time is not enough to significantly alter the concentration profiles inside the membrane. Therefore, after repeated switching the current on (ChP-2), the quasi-steady state of the membrane system is achieved much faster (Fig. 4a, $i = 2.5i_{lim}^{Lev}$) than during the first current pulse (ChP-1). The time for reaching of a short-term quasi-steady state in the case of application of the second pulse (segment III between points *c* and *c*' on ChP-2, Fig. 4b) is approximately 13 s. It is only slightly shorter than that with the first pulse (15 s). However, the potential drop corresponding to this state is noticeably higher for ChP-2 than for ChP-1. This indicates that the time for reaching such a state is determined by the external diffusion of charge carriers. At the same time, the recorded PD is determined by the concentrations and their gradients in the internal boundary solution of the membrane. Since the concentration profiles within the membrane at a time of about 15 s with the repeated current pulse do not differ too much from their shape at the end of the first pulse, the potential drop (approximately 0.35 V) is also closer to its steady-state value (0.7 V), rather than to the value

Table 1. Specific electrical conductivity κ, surface resistance R, and ohmic potential drop on the membrane AX in 0.02 eq/dm^3 solutions of various electrolytes at a current density of 4 mA/cm^2 ($i/i_{lim}^{Lev} = 2.5$)

Electrolyte	κ, mS/cm	R, kΩ cm^2	Δφ, mV
NaH_2PO_4	1.9	0.009	37
Na_2HPO_4	4.5	0.004	18
Na_3PO_4	3.6	0.005	21
NaOH	5.4	0.003	14
NaCl	7.6	0.002	9

corresponding to the attainment of the quasi-steady state on ChP-1 (0.1 V).

During the pause, an inversion in the pH change occurs in both the systems with NaCl and NaH_2PO_4: the pH of the desalting solution decreases when a pulse with a sufficiently high current density is applied, but it increases during the pause. It is obvious that the change in pH is caused by the concentration polarization of the system during the current flow. The mechanism of such changes is described in more detail above. When the external force is eliminated (current is turned off), the system tends to return to its equilibrium state. To completely eliminate the concentration changes in the bulk of the membrane caused by water splitting (AX/NaCl solution system) or the generation of H^+ and HPO_4^{2-} ions (AX/NaH_2PO_4 solution system), a time comparable to the formation of these changes by the action of current is required. In the case of the AX/NaH_2PO_4 solution system, this time is several tens of minutes.

Note that in addition to the phenomena described above, the difference in specific electrical conductivity between membranes in the $H_2PO_4^-$ and HPO_4^{2-} forms can also affect the value of PD and the behavior of ChP. Table 1 shows values for the specific conductivity and surface resistance R of the studied membrane in 0.02 eq/dm^3 solutions of sodium salts of hydrochloric and orthophosphoric acid.

The estimates for the current density of 4 mA/cm^2 (approximately $2.5i_{lim}^{Lev}$) using these data show that when AX is converted from the form of the singly charged anion of orthophosphoric acid to the doubly or triply charged form or to the hydroxyl form, the change Δφ does not exceed 30 mV, with the potential drop decreasing, not increasing as observed in the experiment (Figs. 3, 4). The estimated results confirm that the main effect determining the differences in the behavior of the AX/NaH_2PO_4 solution system compared to the AX/NaCl solution system is the deprotonation of part of $H_2PO_4^-$ ions upon their entry into the membrane (reaction (3)) with the generation of H^+ ions into the depleted solution.

An indirect confirmation of the fact that the proton source in the depleted DL is other than that in the AX/NaCl solution system is the acidification of the depleted NaH_2PO_4 solution at potential drops well below the threshold value of $\Delta\varphi' \approx 0.3$ (Figs. 6a, 6b). It is also noteworthy that for equal exceedances of i_{lim}^{Lev} (by a factor of 2 in Figs. 6a, 6b), the change in the pH of the depleted NaCl solution is much greater than that for the NaH_2PO_4 solution, although the generation rate of H^+ ions in the system with NaH_2PO_4 should be higher, since the contribution of electroconvection in this system is less. The difference in the degree of pH change is explained by the presence of a buffer capacity of the NaH_2PO_4 solution and its absence in the NaCl solution: a significant part of the protons formed at the membrane boundary react with $H_2PO_4^-$ ions to form orthophosphoric acid H_3PO_4 (Fig. 5c). The presence of the protonation–deprotonation products of orthophosphoric acid in the depleted DL leads to a decrease in the PD in the region corresponding to ChP segment II (Fig. 6a) and makes the inflection point b less pronounced (Fig. 6c) in the AX/NaH_2PO_4 solution system compared to the AX/NaCl solution system (Figs. 6b, 6d).

CONCLUSIONS

The transitional section of the chronopotentiogram of the AX/NaH_2PO_4 solution system does not differ qualitatively from that for the AX/NaCl solution system. Above the limiting current density, there is an inflection point, the position of which at $i > 1.5i_{lim}^{Lev}$ agrees with the value of the transition time τ_{Sand} calculated by Eq. (2). The shape of this part of the curve is determined by the electrodiffusion transport of ions in the depleted diffusion layer. As in the case of NaCl, the presence of the inflection point is due to the appearance of additional mechanisms of charge transport: in the general case, this is current-induced convection or the generation of new charge carriers, H^+/OH^- ions. In the system with NaH_2PO_4, coupled convection is less likely at the same i/i_{lim}^{Lev} ratio, since the potential drop in such a system is much smaller, including that at times close to τ_{Sand}. In contrast, the generation of H^+ ions in accordance with equation (3) is more probable, since the deprotonation constant of $H_2PO_4^-$ ions is 3×10^{-2} s^{-1} [27] and is substantially higher than the deprotonation constant of water molecules (2×10^{-5} s^{-1}). The propart of $H_2PO_4^-$ ions that are deprotonated upon their entry into the membrane increases significantly with increasing current density. This is due to a decrease in the electrolyte concentration in the depleted diffusion layer near the membrane

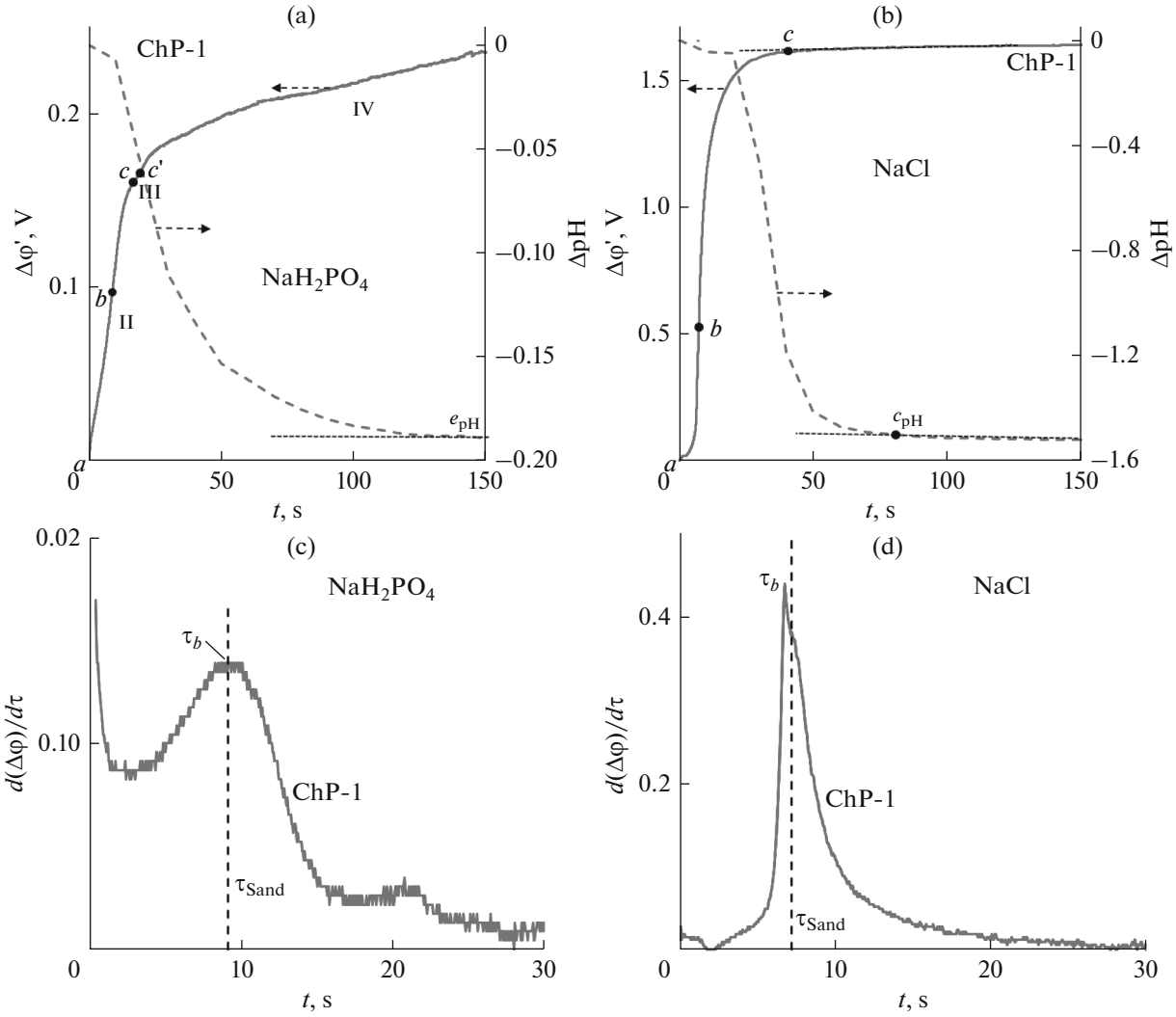

Fig. 6. Reduced chronopotentiograms of the first dc pulse (ChP-1) at $i/i_{lim}^{Lev} = 2$ in the (a, b) common and (c, d) differential forms obtained in 0.02 M solutions of (a, c) NaH_2PO_4 and (b, d) NaCl and (a, b) the corresponding (to the chronopotentiograms) differences in pH at the outlet and inlet of the desalting channels formed by the membrane AX and the auxiliary membrane MK-40.

surface, which entails an increase in the Donnan exclusion of protons from the membrane and an increase in the pH of the internal solution at the boundary with the depleted diffusion layer. The generation of H^+ ions allows the AX/NaH_2PO_4 solution system to reach a short-term quasi-steady state at times comparable with the corresponding times for the system with NaCl. However, at times two- to fourfold longer than τ_{Sand}, the behavior of the AX membrane in the NaH_2PO_4 solution differs substantially from its behavior in the NaCl solution. In the case of NaCl, a steady-state value of the potential drop is established at $t \approx 2\tau_{Sand}$, whereas the potential drop in the case of NaH_2PO_4 continues to grow by about two orders of magnitude with time. This growth is due to concentration changes in the internal solution of the membrane at the boundary with the depleted solution, which propagate throughout the entire volume of the membrane. The process is controlled by internal mutual diffusion of $H_2PO_4^-$ ions and their protolysis products.

The behavior of the system with NaH_2PO_4 at current densities above about $2i_{lim}^{Lev}$ is characterized by an interesting feature. This current density is in a certain sense critical: when it is attained, the concentration of $H_2PO_4^-$ ions in the internal solution of the membrane vanishes to zero, and the membrane volume is saturated with HPO_4^{2-} ions. Under these conditions, the propart of singly charged $H_2PO_4^-$ ions that are deprotonated to HPO_4^{2-} when entering the membrane

reaches 100%. To further increase the concentration of charge carriers, either HPO_4^{2-} deprotonation with the formation of triply charged PO_4^{3-} ions or water splitting with participation of fixed groups at the membrane/solution interface is required. Both of these processes require a higher value of the potential drop in the system. Therefore, under the current flow conditions of $i > 2i_{lim}^{Lev}$, the chronopotentiograms exhibit another inflection point, which appears when a critical value of the potential drop is reached and new charge carriers are generated and is not observed in the case of the NaCl solution.

ACKNOWLEDGMENTS

This work was supported by the Russian Foundation for Basic Research, project no. 15-08-04522_a.

REFERENCES

1. R. He, A. T. Girgih, E. Rozoy, et al., Food Chem. **197**, 1008 (2016).
2. G. Chen, W. Song, B. Qi, et al., Sep. Purif. Technol. **147**, 32 (2015).
3. J. Xu, X.-F. Su, J.-W. Bao, et al., Bioresour. Technol. **189**, 186 (2015).
4. V. A. Shaposhnik and T. V. Eliseeva, J. Membr. Sci. **161**, 223 (1999).
5. T. V. Eliseeva, E. V. Krisilova, V. P. Vasilevsky, and E. G. Novitsky, Pet. Chem. **52**, 609 (2012).
6. M. Metayer, M. Legras, O. Grigorchouk, et al., Desalination **147**, 375 (2002).
7. T.V. Eliseeva and V. A. Shaposhnik, Russ. J. Electrochem. **36**, 64 (2000).
8. V. I. Vasil'eva and E. A. Vorob'eva, Russ. J. Phys. Chem. A **86**, 1852 (2012).
9. E. A. Vorobjeva and V. I. Vasil'eva, Sorb. Khromatogr. Protsessy **10**, 741 (2010).
10. V. Sarapulova, E. Nevakshenova, N. Pismenskaya, et al., J. Membr. Sci. **479**, 28 (2015).
11. P. Ramirez, A. Alcaraz, and S. Mafe, J. Colloid Interface Sci. **242**, 164 (2001).
12. L. Franck-Lacaze, P. Sistat, and P. Huguet, J. Membr. Sci. **326**, 650 (2009).
13. F. Helfferich, *Ionenaustauscher*, Bd. 1: *Grundlagen Struktur-Herstellung-Theorie* (Chemie, Weinheim, 1959).
14. R. Lteif, L. Dammak, C. Larchet, and B. Auclair, Eur. Polym. J. **35**, 1187 (1999).
15. E. D. Belashova, N. A. Melnik, N. D. Pismenskaya, et al., Electrochim. Acta **59**, 412 (2012).
16. V. V. Gil, M. A. Andreeva, N. D. Pismenskaya, et al., Pet. Chem. **56**, 440 (2016).
17. N. P. Berezina, N. A. Kononenko, O. A. Dyomina, and N. P. Gnusin, Adv. Colloid Interface Sci. **139**, 3 (2008).
18. J. S. Newman, *Electrochemical Systems* (Prentice Hall, New York, 1973).
19. N. P. Gnusin, V. I. Zabolotsky, V. V. Nikonenko, and M. K. Urtenov, Russ. J. Electrochem. **22**, 298 (1986).
20. J. J. Krol, M. Wessling, and H. Strathmann, J. Membr. Sci. **162**, 155 (1999).
21. E. D. Belashova, N. D. Pismenskaya, V. V. Nikonenko, et al., J. Membr. Sci. **542**, 177 (2017). doi.org/10.1016/j.memsci.2017.08.002
22. H. Roques, *Fondements théoriques du traitment chimique des eaux*, in two vols. (Lavoisier, Paris, 1990).
23. D. R. Lide, *CRC Handbook of Chemistry and Physics* (CRC, Boca Raton, 1995).
24. N. Pismenskaya, E. Laktionov, V. Nikonenko, et al., J. Membr. Sci. **181**, 185 (2001).
25. N. Pismenskaia, P. Sistat, P. Huguet, et al., J. Membr. Sci. **228**, 65 (2004).
26. S. A. Mareev, D. Yu. Butylskii, N. D. Pismenskaya, and V. V. Nikonenko, J. Membr. Sci. **500**, 171 (2016).
27. V. I. Zabolotsky, N. V. Sheldeshov, and N. P. Gnusin, Russ Chem. Rev. **57**, 501 (1988).
28. E. I. Belova, G. Yu. Lopatkova, N. D. Pismenskaya, et al., J. Phys. Chem. B **110**, 13458 (2006).
29. N. D. Pismenskaya, V. V. Nikonenko, E. I. Belova, et al., Russ. J. Electrochem. **43**, 307 (2007).
30. L. A. Zagorodnykh, O. V. Bobreshova, P. I. Kulintsov, and I. V. Aristov, Russ. J. Electrochem. **42**, 59 (2006).
31. I. Rubinstein and B. Zaltzman, Phys. Rev. E: Stat. Phys., Plasmas, Fluids, Relat. Interdiscip. Top. **62**, 2238 (2000).
32. I. Rubinstein, B. Zaltzman, A. Futerman, et al., Phys. Rev. E: Stat. Phys., Plasmas, Fluids, Relat. Interdiscip. Top. **79**, 021506 (2009).
33. E. A. Shutkina, E. E. Nevakshenova, N. D. Pismenskaya, et al., Kondens. Sredy Mezhfaz. Granitsy **17**, 566 (2015).

Translated by S. Zatonsky